Journal of Quantitative Spectroscopy & Radiative Transfer 112 (2011) 236–246

Contents lists available at ScienceDirect

Journal of Quantitative Spectroscopy & Radiative Transfer

journal homepage: www.elsevier.com/locate/jqsrt

The primary design of advanced ground-based atmospheric microwave sounder and retrieval of physical parameters

He Jie Ying [a,b,*], Zhang Sheng Wei [a], Zhang Yu [a,b]

[a] Center for Space Science and Applied Research, Chinese Academy of Sciences, China
[b] Graduate University of Chinese Academy of Sciences, Beijing, China

ARTICLE INFO

Keywords:
Ground-based
Microwave sounder
Direct detect type
Temperature profiles
ANN

ABSTRACT

This paper introduces a prototype of ground-based atmospheric microwave sounder that operates in K-band from 22 to 31 GHz and V-band from 51 to 59 GHz. Different from the MP3000A and RPG, the sounder adopts independent dual-band reflectors instead of sharing a dual-band reflector. The direct detect type receiver is applied, which is of smaller size, higher sensitivity, efficient data observing and lower nonlinear error than the widely used superheterodyne receiver. The observing brightness temperatures from this prototype agree well with the simulated brightness temperatures according to the ground-based radiative transfer theory. We use the artificial neural network (ANN) algorithm to retrieve temperature profiles, which has higher spatial resolution especially in the capping inversion when compared with the linear regression algorithm. The temperature retrievals are comparable with the retrievals from RPG and MP3000A retrieval models and have a smaller bias in some certain regions.

1. Introduction

Atmospheric temperature is one of the most important meteorological parameters. There are two traditional sounding instruments to retrieve temperature profiles: radiosonde (radar) working on the ground and remote sensing satellite working on a high spatial orbit. The former one is bulky and costly perplexing to install and operate, and has lower spatial and temporal resolution. The latter one has higher spatial resolution and wider coverage. However, due to the shelter and strong absorption of cloud, as well as atmospheric opacity for electromagnetic wave in the millimeter-wave band, satellite instrument with limitation of remote sensing technology has a lower vertical resolution at the bottom of troposphere.

In recent years, ground-based atmospheric microwave sounder has been operated widely to retrieve temperature profiles and other parameters. Compared with radiosonde (radar), ground-based atmospheric microwave radiometer can be operated in a long-term unattended mode under almost all weather conditions with reliable results and has a low maintenance cost. Compared with remote sensing satellite, ground-based atmospheric microwave radiometer has a high resolution at the bottom of lower troposphere. With the long-term development of theory and laboratory measurements, it has been used in meteorological observations and forecasting, communications, geodesy and long-baseline interferometry, satellite validation, climate and fundamental molecular physics.

Currently, MP3000A of USA and RPG of Germany are the main ground-based atmospheric microwave sounders to sound temperature profiles and related parameters [1,2]. Both of them have mature techniques and have been used in many regions. Also, they have complete data-processing software to retrieve temperature profiles and other important parameters.

* Corresponding author at: National Microwave Remote Sensing Laboratory, Center for Space Science and Applied Research, Chinese Academy of Sciences. D.O. Box: Beijing 8701, No.1 Nanertiao, Zhongguancun, Haidian district, Beijing 100190, China. Tel.: +86 10 62632256; fax: +86 10 62576921.
E-mail address: peggy.hejieying@163.com (H. Jie Ying).

0022-4073/$ - see front matter © 2010 Elsevier Ltd. All rights reserved.
doi:10.1016/j.jqsrt.2010.05.021

With the development of retrieval techniques, there are mainly two algorithms. (1) Linear regression algorithm, which is simple and has clear representation of physical parameters, stable levels of results and high accuracy. Guiraud gave the regression equation to retrieve water vapor density in 1998 [3]. F.D. Frate used microwave radiometer of 7 channels to improve the accuracy of temperature and humidity profiles [4]. (2) Nonlinear regression algorithm, such as artificial neural network, which has been widely used in the retrievals of microwave radiometers. Churnside et al. [5] in 1994 successfully retrieved the temperature profiles using artificial neural network (ANN) with 3 layers. Fredrick Solheim et al. used artificial neural network and other retrieval methods to retrieve temperature profiles and humidity profiles successfully in 1998 [6]. Yao et al. [7] in 2005 demonstrated back propagation artificial neural networks can significantly improve the temperature retrievals in all the weather conditions comparing with the IAPP model, especially at the lower levels. RPG-HATPRO and MP3000A series also constructed retrieval models using neural network algorithm to derive temperature and humidity profiles with high accuracy [1,8,9].

The Advanced Microwave Sounding Unit-A (AMSU-A) is the latest microwave temperature sounder of the new generation polar orbiting satellite operated by the National Ocean and Atmospheric Administration (NOAA). The first AMSU-A sounder aboard the NOAA-15 satellite was launched on May 13, 1998. In the following years, more and more researchers used different retrieval algorithms with AMSU-A datasets from different NOAA satellites. Yao et al. [7] used back propagation artificial neural networks to retrieve atmospheric temperature profiles from NOAA-16 Advanced Microwave Sounding Unit-A (AMSU-A) measurements over East Asia.

In this paper, we mainly introduce a prototype of advanced ground-based atmospheric sounder with improvements. In this prototype, the receiver system adopts direct detect type rather than superheterodyne type, which is used in almost all the microwave radiometers recently. For the reflector configuration, it adopts two independent reflectors in each band rather than sharing one reflector in dual band. Also we construct retrieval models of temperature profiles using artificial neural network and linear regression algorithm. By comparing the algorithms between linear regression and artificial neural network, we can choose the better retrieval algorithm. Compared to the retrieval experiments using artificial neural network like RPG-HATPRO [7,8] and MICCY [10], the results show that the retrieval model is correct and has better retrieval accuracy in some regions partly. Experimental results on several datasets from different regions and different seasons demonstrate that the instrument can be operated commonly in different regions and climates and achieve high quality temperature profiles.

2. Advanced techniques of prototype

Referred to MP3000A, we propose an advanced prototype of atmospheric microwave sounder with similar specifications (shown in Table 1) in the aspects of calibration resolution, stability, brightness temperature range, antenna resolution and side lobe, integral time, water vapor and oxygen channels and bandwidth. However, compared with the MP3000A, our prototype has several improved techniques mainly in the receiver and reflector configuration as follows.

Table 1
Comparison of specifications between the prototype and MP3000A.

Specification	Prototype of design	MP3000A
Calibration resolution	1.5k	$0.2+0.002^{*}\lvert TkBB-Tsky\rvert$
Long-term stability	<1.0k/year	<1.0k/year
BT resolution	0.1–1k	0.1–1k
BT coverage	0–400K	0–400K
Antenna resolution and side lobe		
22–30 GHz	$4.9–6.3^{\circ}$ -24 dB	$4.9–6.3^{\circ}$ -24 dB
51–59 GHz	$2.4–2.5^{\circ}$ -27 dB	$2.4–2.5^{\circ}$ -27 dB
International time	0.01–2.5 s	0.01–2.5 s
Water vapor channel	22–30 GHz (>7 channels)	22–30 GHz (21 channels)
Oxygen channel	51–59 GHz (>7 channels)	51–59 GHz (14 channels)
Bandwidth	300M	300M

2.1. Radiometer receiver

With current techniques, the receiver of ground-based atmospheric microwave sounder mainly has two types: superheterodyne type with mixer and RF direct detect type without mixer. Their schematic diagrams are shown in Figs. 1 and 2, respectively.

In Fig. 1, the former system of receiver is used in MP3000A. The antenna and feedback unit accepts microwave radiation of atmosphere and internal calibration source. Then the receiver amplifies RF signal and completes the down-conversion from RF signal to IF, and then the IF signals are amplified, detected and integrated. Finally the signal is quantified and processed in the digital control unit.

On the other hand, in Fig. 2, the receiver operates in direct detect type, which is adopted by the present prototype. Microwave radiometer receiver with direct detect type mainly consists of directional coupler, RF amplifier, power divider, band-pass filter, square law detector, integrator and video frequency amplifier. The signal accepted by the antenna is amplified and distributed into several RF channels without mixers. It uses the band-pass filter to decide the frequency for each channel. Here the bandwidths in different channels can be different. In the system, the number of sounding-channel depends on power divider network. Different from the superheterodyne type, it is easy to control and operate without mixer and frequency synthesizer.

In our study center, in order to prove the advancements of direct detecting receiver, we have designed a direct detect type receiver whose frequencies are 18.7 and 36.5 GHz. For a valuable comparison, a superheterodyne type receiver whose frequencies are 19.35 and 37 GHz is also designed by our center. They have similar specifications and are comparable in many aspects as shown in Table 2.

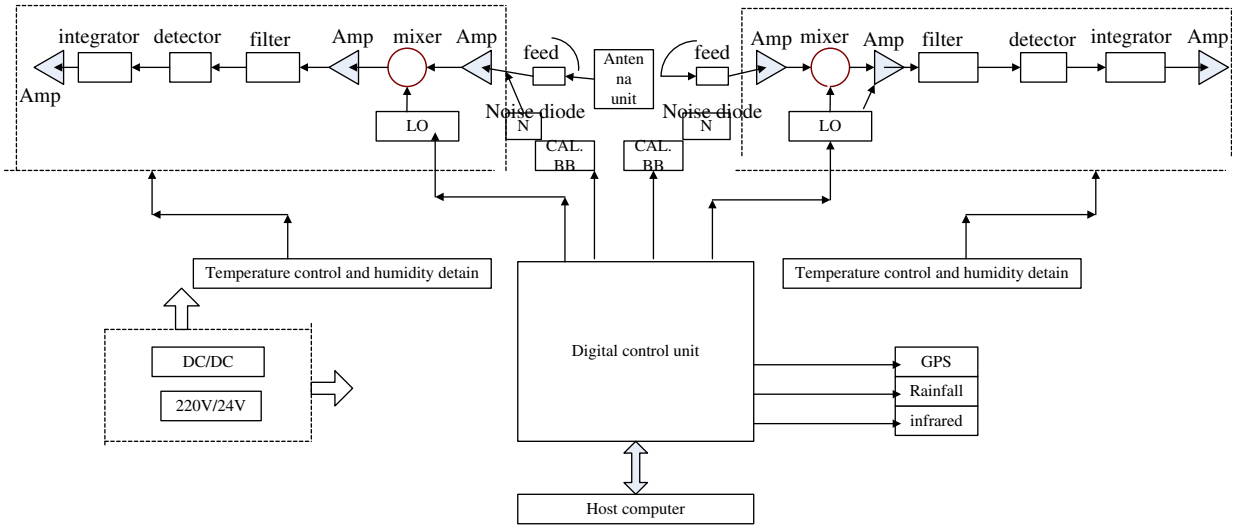

Fig. 1. Superheterodyne type receiver. In the microwave sounder of MP3000A, the receiver adopted this mode.

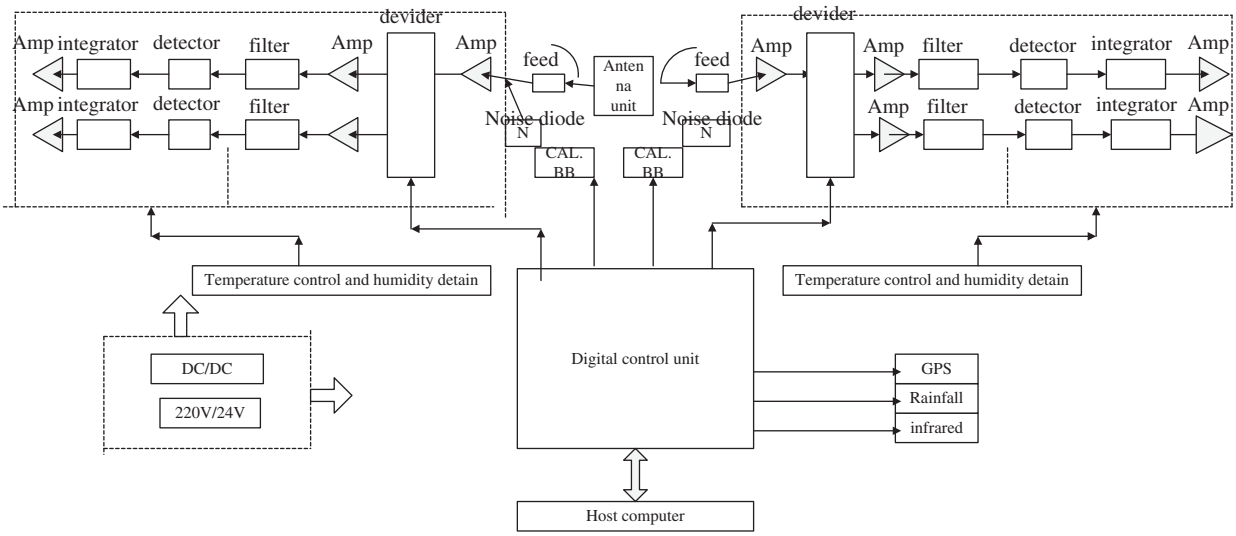

Fig. 2. Direct detect type receiver. In the present prototype of ground-based atmospheric microwave sounder, the receiver adopts this mode.

So obviously the receivers in direct detect type have the following advantages:

(1) no mixer sideband filtering requirements and LO drifts;
(2) no frequency down conversion, so reducing the interference of external signals;
(3) simultaneous measurements of all frequency channels and high temporal resolution;
(4) small size and weight and low loss.

Based on a similar principle, we designed the prototype of ground-based microwave atmospheric sounder with a direct detecting receiver, and compared to MP3000A, it has the above advantages, too. The characteristics of direct detect type and superheterodyne receivers are listed in Table 3.

In addition to these common advantages, the receiver of direct detect type has an effect on retrieving temperature profiles. Because the receiver of this type has an efficient observation that can observe all channels synchronously, the prototype has a high system resolution. Using brightness temperature measurements from this prototype, this paper retrieves atmospheric profiles with high accuracy with little influence of temporal and spatial difference. Therefore the retrievals from this prototype are in good agreement with the radiosonde datasets.

2.2. Configuration

The configuration of MP3000A has a sharing reflector and the configuration mode is shown in Fig. 3. Based on the deployment of FY-3 microwave humidity sounder [11], the

Table 2
Comparison between two types.

Indicators	System			
	Superheterodyne		Direct detect〈H/V〉	
Frequency〈GHz〉	19.35	37	18.7	36.5
Bandwidth〈MHz〉	400	500	500	600
Integral time〈ms〉	200	200	200	200
Resolution〈k〉	0.13	0.2	0.17/0.18	0.12/0.16
Linearity	0.99979	0.99984	0.99969/0.9996	0.99989/0.99970
Nonlinear error	0.2	0.25K	0.3/0.25	0.1/0.2
Power consumption (W)	3.0	3.0	2.5	2.8
Weight〈kg〉	1.4	1.1	0.85	0.70
Size〈mm^3〉	$180\times100\times40$	$170\times86\times37$	$120\times70\times45$	$108\times70\times42$

Table 3
Respective characters of two types of receivers.

Content	Direct detecting type	Superheterodyne type
Components	Filter bank+multi-channels detecting	LO+single RF+IF+LF
Structure	Simple	Complex with mixer and LO
Number of channels	Smaller, realized by power divider	Fixed, realized by LO frequency-splitter
Configuration of channels	Fixed, depend on number of filters and detectors	Flexible, depend on the number of splitter times
Efficiency of measurement	High, measure multi-channels simultaneously	Low, measure one channel at each time

prototype of ground-based atmospheric microwave sounder adopts independent antenna and feedback in K- and V-band, respectively, so in each band there is a reflector and the configuration mode is shown in Fig. 4.

The type of sharing a reflector needs additional space for mounting a polarized grid. Also it has a larger height value and has a width nearly equal to that of the second mode, which has independent reflectors. Therefore it has a larger size than the second mode. However, adopting independent reflectors, we can design and optimize them independently and also make the width of antenna as small as possible. With a smaller height value and a similar width value, we can decrease the whole size and whole device expense.

The real size of MP3000A is $500\times280\times760\ mm^3$ and the power consumption is 400 W, while in the prototype, the size is $400\times350\times880\ mm^3$ and the power consumption is 800 W. In additional to the smaller size, the two independent reflectors configuration mode actually avoids the problems caused by the polarized grid as follows:

(1) processing difficulty and high cost;
(2) system consumption and difficulty in improving sensitivity;
(3) improving accuracy difficulty, because the antenna reflector has to balance the difference between high and low frequencies;
(4) having strict specification restriction, because the radome and calibration blackbody have to balance dual-band frequencies.

To overcome the disadvantages above, the prototype adopts two independent reflectors. In this configuration mode, we can easily release the low sidelode and design the antenna in dual band independently without frequency segregation. The prototype has high calibration accuracy because it uses independent blackbody in each band and need not consider the dual band requirements. Furthermore, it decreases the wave loss through radome and has high expansibility to release multi-polarization measurements.

3. Sounding principle

Ice, cloud, rain snow, etc. play an important role in attenuation in the atmosphere sounding of microwave radiometer. All of them are caused by atmospheric temperature and humidity. So the brightness temperature is related to atmospheric temperature and humidity, and given the brightness temperature we can retrieve the vertical distribution of atmospheric temperature profiles and other parameters.

The principle of atmospheric temperature sounding is to measure the atmospheric (oxygen and water vapor) molecular rotating absorbing spectrum and its wings, all of which are pressure broadened. The oxygen molecular absorbing spectrum at about 50–60 GHz can be used for retrieving temperature profiles and water molecular absorbing spectrum at about 20–30 GHz for retrieving humidity profiles. Given the brightness temperature from the observations or radiative transfer equation, we can complete the retrieval of temperature and humidity profiles.

Fig. 5 shows the high opacity of atmosphere microwave attenuation coefficients (oxygen and water vapor) using the US standard atmospheric profile. Both of them play an important role in calculating brightness temperature, especially the oxygen absorption coefficients in sounding atmospheric temperature profiles. This paper considers the influence of both factors. In the band of 0–200 GHz, there are two lines of oxygen (detecting atmospheric temperature profiles) and water vapor (detecting atmospheric humidity profiles). The energy spectrum enhances gradually as the frequency becomes higher and higher. The oxygen lines are at 50–60 GHz (usually measures space-borne vertical distribution of atmospheric oxygen) and 118 GHz. The

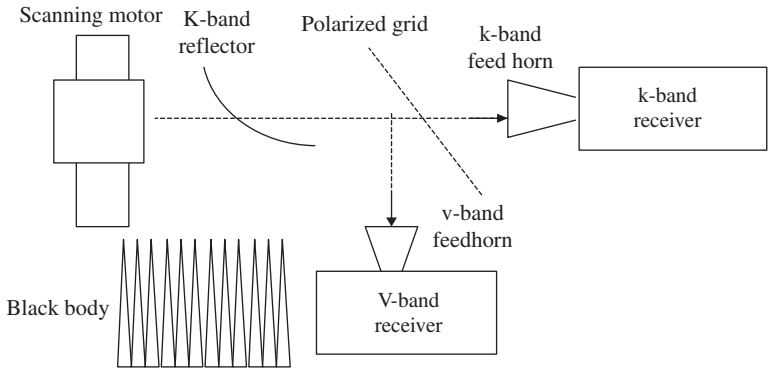

Fig. 3. Configuration mode adopted by MP3000A, which is produced by USA (Sharing one reflector).

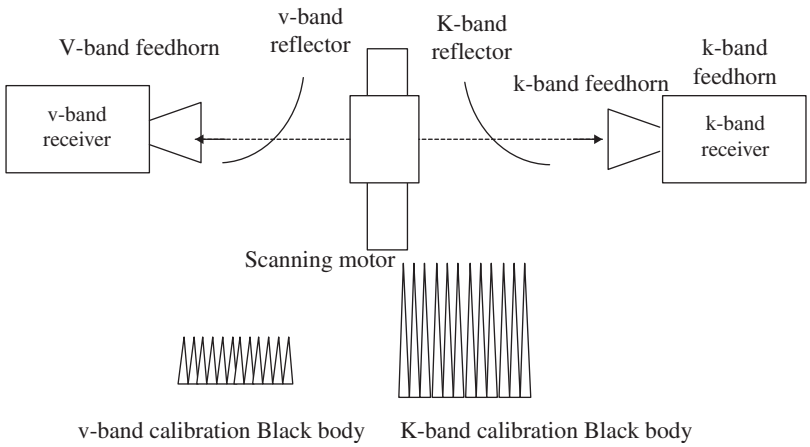

Fig. 4. Configuration mode with independent reflectors, which is adopted by the present prototype.

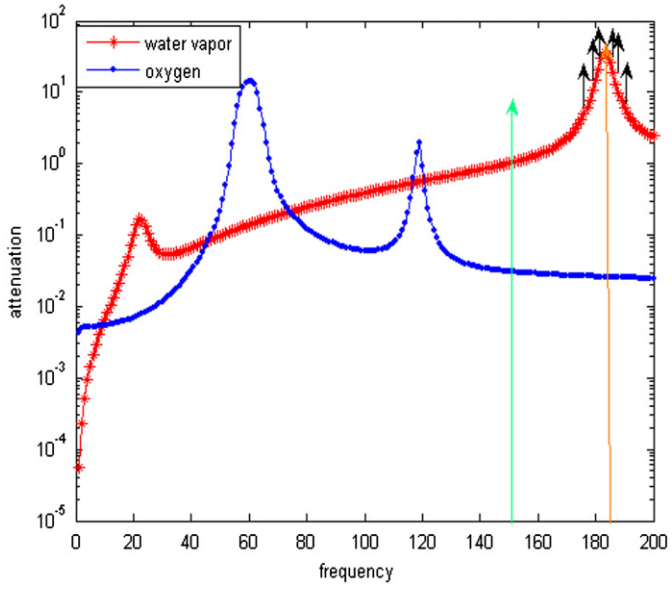

Fig. 5. Opacity of atmosphere microwave transmission, which is calculated using the Ulaby's coefficients and US standard atmosphere.

water vapor lines are at 22.235 and 183.31 GHz. The former line has low atmosphere attenuation and is partly transparent, which can be used to measure water vapor content, and the latter one can be used for measuring vertical distribution of space-borne high-altitude atmospheric water vapor profiles [12].

Having the same principle as and referring to MP3000A, the ground-based atmospheric microwave radiometer operates at K-band (22–31 GHz) and V-band (51–59 GHz), and retrieves the atmospheric temperature profiles, humidity profiles and other related parameters like liquid water vapor, flux, delay, etc.

Using radiative transfer equation and atmospheric absorption model [13], according to Eqs. (1)–(5), we can derive weighting functions of temperature profiles. Based on radiosonde datasets, we can calculate the brightness temperature of different channels at different frequencies.

The Fredholm integral equation of the first kind is as follows:

$$T_b = \int_0^{\infty} T'(s)\alpha(s)e^{-\tau(0,s)}ds + T_{b0}e^{-\tau(0,\infty)} \tag{1}$$

$$T'(s) = T(s)/R[T(s)] \tag{2}$$

$$R(T) = \frac{kT}{h\nu}(e^{h\nu/kT}-1) \tag{3}$$

$$\text{Optical thickness}: \quad \tau(s_1,s_2) = \int_{s_1}^{s_2} \alpha(s')ds' \tag{4}$$

$$\text{Weighting function}: \quad W_T(s) = \alpha(s)\exp\left[-\int_0^{s} \alpha(s')ds'\right] \tag{5}$$

where T_b denotes brightness temperature at the top of atmosphere, T denotes the temperature profiles, $\alpha(s)$ denotes the atmospheric attenuation coefficients, T_{b0} denotes surface temperature, h is Plank's constant, k Boltzmann's constant, and s denotes the height of different atmospheric layer.

4. Retrieval algorithms

4.1. Artificial neural network

In recent years, back propagation artificial neural network (ANN) has been used widely, which has retrieved temperature profiles with high accuracy [14,15]. ANN is essentially a nonlinear statistical regression between a set of predictors—in this case the observation vectors X, and a set of predictands—in this case profiles of atmospheric temperature Z. The structure of ANN is shown in Fig. 6. The layers 1–3 represent the input layer, the hidden layer and the output layer, respectively. The neurons of the input layer are represented by vector X_i ($X_1, X_2, X_3, \ldots, X_L$), where L is the number of input neurons. The neurons of the middle layer are represented by vector Y_i ($Y_1, Y_2, Y_3, \ldots, Y_M$), where M is the number of hidden neurons. The neurons of the output layer are represented by vector Z_i ($Z_1, Z_2, Z_3, \ldots, Z_N$), where N is the number of output neurons.

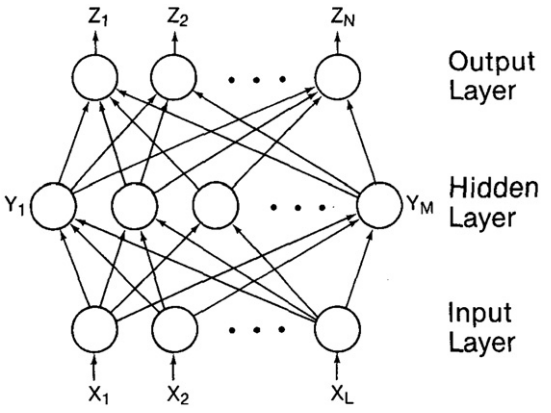

Fig. 6. Schematic diagram of a three-layer back-propagation neural network, including one input layer, one hidden layer and one output layer, L, M and N denote the number of their neurons, respectively.

For the jth node in the hidden layer, this can be expressed as

$$Y_j = S\left(\sum_{i=1}^{L} w_{ij}x_i + b_j\right) \tag{6}$$

where S denotes the sigmoid function:

$$S(\alpha) = \frac{1}{1+\exp(-\alpha)} \tag{7}$$

Here w_{ij} is the weighting of the connection between the jth hidden neuron and the ith input neuron and b_j denotes the bias in the jth neuron of the hidden layer. The Purelin linear function is applied between the output layer and the hidden layer. As a result, the output values can be arbitrary in the range [0,1]. The neuron of the output layer can be expressed as

$$Z_k = \sum_{j=1}^{M} w_{jk}Y_j + b_k \tag{8}$$

where w_{jk} is the weight of the connection between the jth hidden neuron and the kth output neuron; b_k is the bias in the kth neuron of the output layer.

4.2. Linear regression algorithm

According to the radiative transfer equation, the forward model can be expressed as

$$y = F(x) \tag{9}$$

where y denotes the observation vector, and x denotes the atmospheric parameter vector. Then x can be retrieved using the following equation:

$$\hat{x} = R(y+\varepsilon) \tag{10}$$

Using the radiosonde datasets, we construct the linear regression model [16]

$$x = a + bY \tag{11}$$

where x and Y denote the temperature profile and known parameters, respectively. Suppose there are n layers in the atmosphere; then x is an $n\times 1$ vector and Y is

an $m\times 1$ dimensional vector. Then

$$X = AY \tag{12}$$

where X is the regression matrix in the linear regression of radiosonde datasets.

In the experiment, X denotes the temperature profile distributed at 50 height values of atmosphere, and Y denotes the brightness temperatures of 7 sounding channels and surface temperature, humidity and pressure. Using the radiosonde datasets we can derive the regression matrix A, and then retrieve the temperature profiles in different regions and at different times.

5. Retrieval datasets and retrieval results

According to the description of introduction, the algorithm of ANN has to decide the number of neurons in input layer, hidden layer and output layer. In this paper, the input has 10 neurons including 7 brightness temperatures of 7 different channels with different frequencies, surface temperature, surface pressure and surface humidity. We choose 10 neurons in hidden layers and 50 neurons in output layers including 50 temperatures in different pressure values. So the output values can define the temperature profiles [17].

Due to the different absorption coefficients of oxygen and water vapor at different pressures and heights, during the retrieval process of physical parameters, the distribution of weighting function is variable and critical. In the simulation experiment of clear air, the weighting function is as shown in Fig. 7.

The neural network to be tested here was trained on a set of 1 year (2008) of radiosonde profiles from Beijing (54511, 116.28° in longitude and 39.93° in latitude) and RJAO station (47971, 142.18° in longitude and 27.08° in latitude) at 00z and 12z. For the radiosonde datasets, they provide the profiles of temperature, mixer ratio of water vapor, pressure, height and relative humidity. Then these profiles are processed at discrete levels every 200 m up to 10 km. Although the number of independent measurements is only 50 levels output, this sampling ensures the retrieval profiles can be accurately represented on the fixed levels. The profiles are then put into the radiative transfer model to synthesize the brightness temperatures as simulated values and derive the temperature weighting functions of different channels in the zenith position. We calculate the oxygen absorption and water vapor absorption coefficients according to the MPM 93 model. Also, the absorbing coefficients can be calculated from Rosenkranz [18] in K-band, and Liebe [19] in K- and V-bands. Here, the surface temperature, surface pressure and relative humidity are also directly connected. Gaussian noises of 0.5k are added in the temperature profiles. This extends the training datasets slightly and reduces the sensitivity of the network to noise in the data and can represent all the errors affecting the observations.

According to Eq. (5) and radiosonde parameters from the datasets we choose, the temperature weighting functions of different channels can be simulated. Fig. 7 shows the relationship between weighting functions and height, which is significant in calculating brightness temperatures of different channels.

Due to the constraint of atmospheric layers of radiosonde datasets and other influent factors like region, climate and weather, the temperature weighting functions have large variability. First, excluding the cloudy, rainy and other extreme weathers, in clear air, using the artificial neural network retrieval model, which is

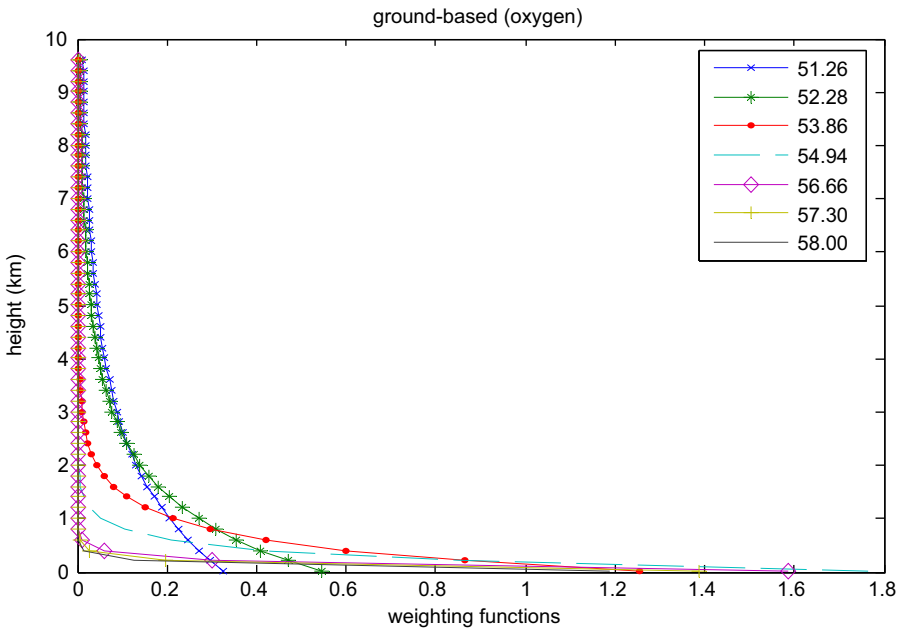

Fig. 7. Normalized temperature-weighting functions; the frequencies are 51.26, 52.28, 53.86, 54.94, 56.66, 57.30 and 58.00 GHz; different annotations denote different channels.

constructed successfully, we retrieve the temperature profiles in 50 isothermal layers in the stations 47971 and 54511. The results are shown in Figs. 8 and 9. Fig. 8 shows a comparison between temperature profiles from artificial neural network model and radiosonde datasets, which can be used to calculate brightness temperatures according to atmospheric radiative transfer model. It also shows the temperature bias of retrievals using the artificial neural network retrieval model. Fig. 9 shows one dataset of those retrievals and bias.

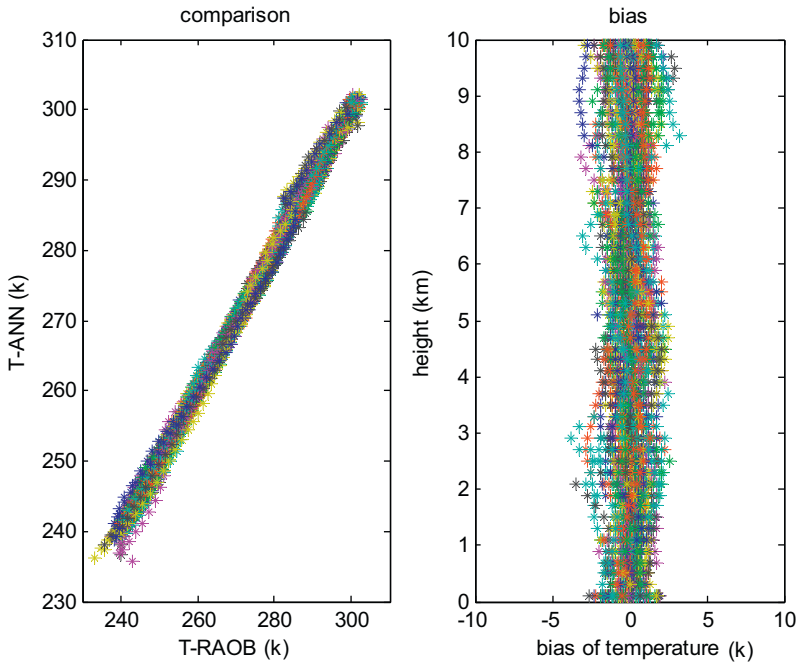

Fig. 8. Comparison and bias of temperature profiles between ANN retrievals and radiosonde datasets.

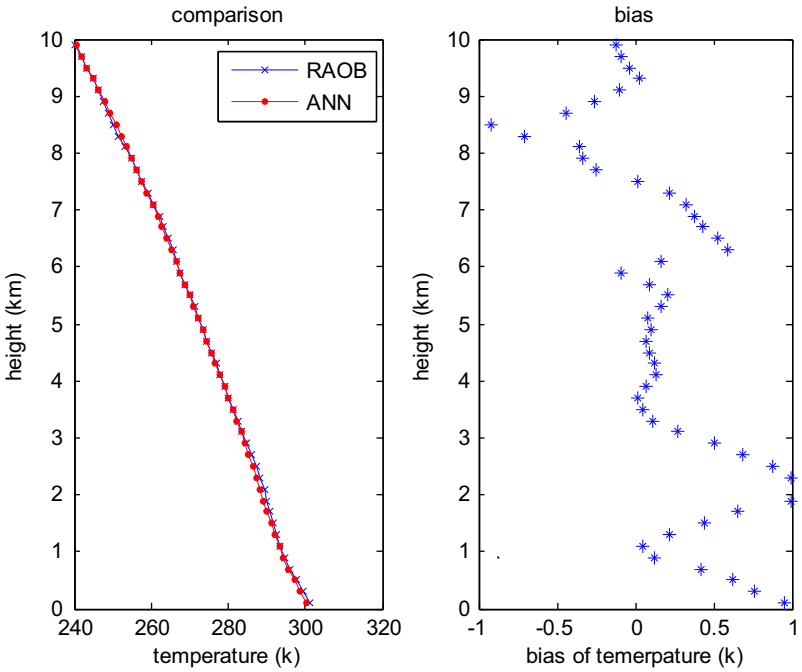

Fig. 9. One set of comparison and bias of temperature profiles between ANN retrievals and radiosonde datasets.

Second, using the same datasets used in the artificial neural network model, we retrieve temperature profiles using linear regression algorithm as described in Section 4, and the results are shown in Figs. 10 and 11. Fig. 10 shows the comparison between retrieval temperatures using linear regression algorithm and radiosonde profiles and shows the temperature bias of retrievals using the linear regression algorithm. Fig. 11 shows one set of comparison and bias of temperature profiles between linear regression retrievals and radiosonde datasets.

Comparing the results using artificial neural network and linear regression algorithms, we can see that both

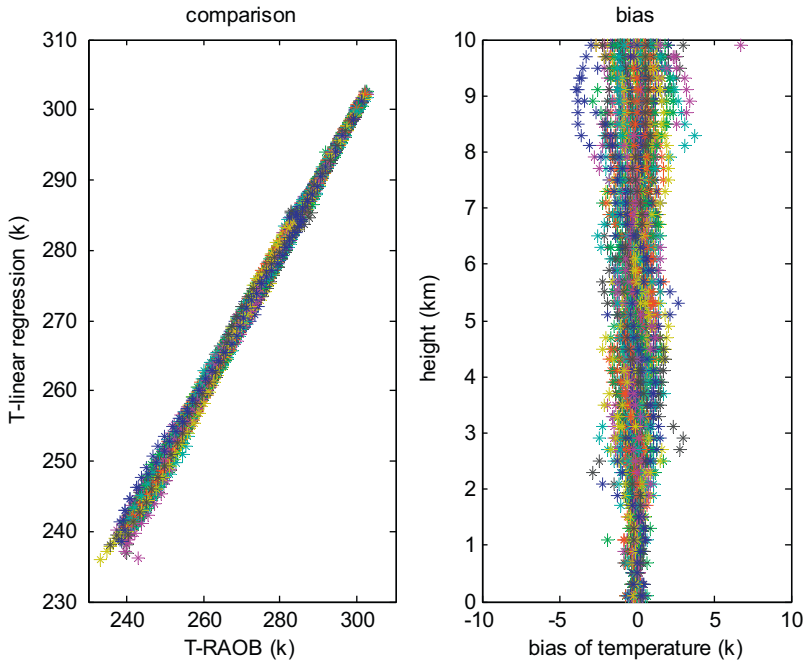

Fig. 10. Comparison and bias of temperature profiles between linear regression retrievals and radiosonde datasets.

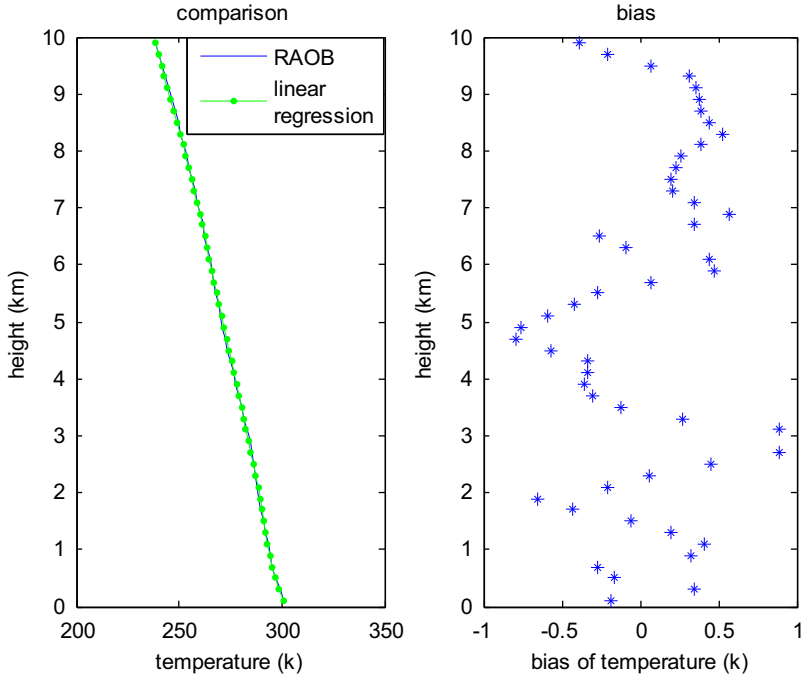

Fig. 11. One set of comparison and bias of temperature profiles between linear regression retrievals and radiosonde datasets.

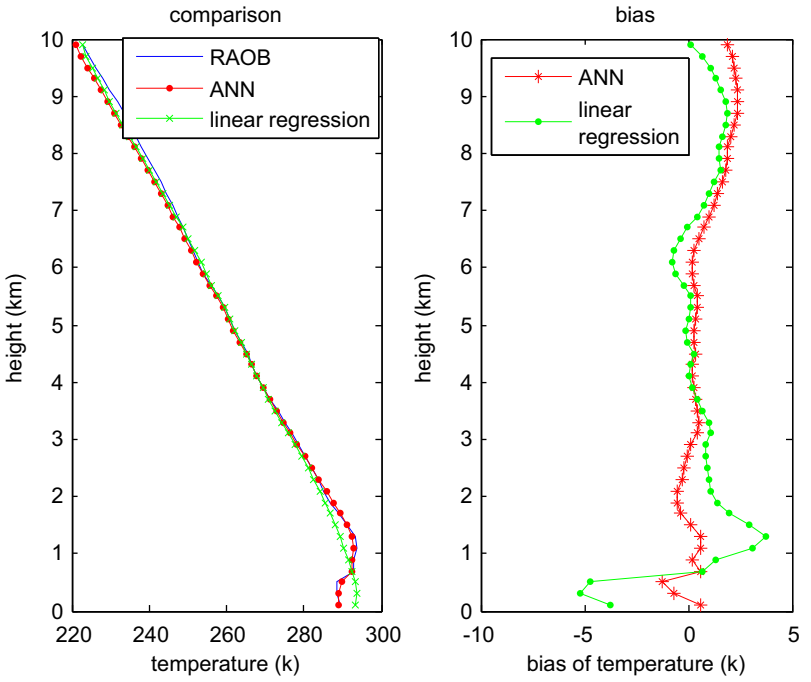

Fig. 12. Comparison and bias of temperature profiles among radiosonde, neural network model and linear regression model in the capping inversion.

algorithms can retrieve atmospheric temperature profiles with accessible biases. In some conditions, the results using linear regression algorithm are better than those from artificial neural network, like the comparison shown in Figs. 9 and 11. But in other conditions, this conclusion may not be correct. Fig. 12 shows an example of this condition. It shows comparison of retrievals among radiosonde, ANN and linear regression algorithm shows that in the capping inversion, the temperature profiles using neural network algorithm agree well with the radiosonde profiles rather than those of the linear regression algorithm. Given sufficient training datasets include all test conditions and sufficient training time, the results show that neural network is better than linear regression. So in the actual work we must consider all the conditions and choose a suitable algorithm to retrieve the atmospheric temperature profiles.

6. Conclusions

The primary design of an advanced ground-based atmospheric microwave sounder has similar specifications as those of MP3000A. But according to the experiments and measurements, it has the advantages of small size and weight, low cost, low maintenance cost, processing data easily, high efficiency and high sensitivity due to the adoption of a direct detect type receiver and two independent reflectors in dual band. Compared with linear regression method, artificial neural network is slow in training, but it is very fast in performing retrievals. However, as with any nonlinear regression methods, neural networks are prone to generate erroneous results if applied outside the range of the training datasets. After completing training process, the model can successfully retrieve accurate temperature profiles stably and efficiently and has a smaller bias, especially in the capping inversion. Due to the characteristic of nonlinear relationship, output results from the ANN model are closer to the actual atmospheric condition. Compared to the temperature retrieval with PRG-HATPRO data using neural network algorithm [7,8], the prototype has a comparable ability to derive temperature profiles. Furthermore in the stations 47971 and 54511, the bias is smaller in the simulation model and has an improvement of a fraction of Kelvin. Compared with the temperature retrieval with AMSU-A data using neural network algorithm, the present prototype can retrieve temperatures with higher accuracy in the low altitude, especially at the bottom of the troposphere with an improvement of a fraction of Kelvin. So this paper demonstrates that the prototype can be operated successfully and efficiently in aspects of meteorology, astronomy, geodesy, communication, traffic, agriculture, and so on. In future, we will continue to improve the retrieval algorithm to derive temperature profiles with higher resolution and combine the satellite-based and ground-based instruments to retrieve more accurate temperature profiles.

Acknowledgements

The work presented in this paper was sponsored by the China Meteorological Administration nonprofit sector (meteorology) Special Research and Grant Nos. GYHY200906035 and 863 High-Techs 2007AA120701.

References

[1] MP-Series Microwave Profilers. Operating manual. Radiometrics Corporation, 2008. 〈http://www.radiometrics.com/MP_Specifications_7-3-07.pdf〉.

[2] RPG-150-90/RPG-DP150-90 high sensitivity LWP radiometers, RPG's atmospheric remote sensing radiometers. Operating manual. Radiometer Physics GmbH, version 7.50, 2008, 〈http://www.radiometer-physics.com〉.

[3] Guiraud FO, Howard J, Hogg DC. A dual-channel microwave radiometer for measurement of precipitable water vapor and liquid. IEEE Transactions on Geoscience Electronics 1979;17(4):129–36.

[4] Del Firate F, Schiavon G. A neural network algorithm for the retrieval of atmospheric profiles from radiometric data. Geoscience and Remote Sensing, IEEE 1997:2097–8.

[5] Churnside, JH, Stermitz, TA, Schroeder, JA. Temperature profiling with neural network inversion of microwave radiometer date. Journal of Atmospheric and Oceanic Technology 1994;11(1):105–9.

[6] Solheim Fredrick, Godwim John R. Radiometric profiling o temperature, water vapor and cloud liquid water using various inversion methods. Journal of Radio Science 1998;33(2):393–404.

[7] Yao Zhigang, Chen Hongbin, Lin Longfu. Retrieving atmospheric temperature profiles from AMSU-A data with neural networks. Advances in Atmospheric Sciences 2005;22(4):606–16.

[8] Th. Rose H. Czekala, RPG-HATPRO, RPG-TEMPRO, RPG-HUMPRO humidity and temperature profilers, operating manual, 2006.

[9] Th. Rose H. Czekala, Accurate atmospheric profiling with the RPG-HATPRO humidity and temperature profiler, operating manual. PRG Meckenheim, Germany, 2005.

[10] Crewell Susanne, Czekala Harald, Lohnert Ulrich, Thomas Rose Clements Simmer, Zimmermann Ralf, Zimmermann Rudiger. Microwave radiometer for Cloud carthography: a 22-channel ground-based microwave radiometer for atmospheric research. Journal of Radio Science 2001;36(4):621–38.

[11] Zhang Sheng-wei, Li Jing, Jiang Jing-shan, Sun Mao-hua, Wang Zhen-zhan. Design and development of microwave humidity sounder for FY-3 meteorological satellite. Journal of Remote Sensing 2008;12(3):199–207.

[12] Ulaby Fawwaz T, Moore Richard K, Fung Adrian K. In: Microwave remote sensing (I). New York: Addison-Wesley Publishing Company; 1982.

[13] Jansssen Michael A. In: Atmospheric remote sensing by microwave radiometry. Wiley-Interscience; 1995.

[14] Lei Shi. Retrieval of atmospheric temperature profiles from AMSU—a measurement using neural network approach. Journal of Atmospheric and Oceanic Technology 2001;18(3):340–7.

[15] Ge Zhexue, Sun Zhiqiang. In: Neural network principles and MATLAB R2007 application. Publishing House of Electronics Industry; 2007.

[16] Bo Wang, Research on remote sensing atmospheric environment measured by ground-based microwave radiometer. PhD thesis, China Institute of Radio Propagation, 2007.

[17] Churnside Jamess H, Stermitz Thimas A, Schroeder Judith A. Temperature profiling with neural network inversion of microwave radiometer data. Journal of Atmospheric and Oceanic Technology 1994;11(1):104–9.

[18] P.W. Rosenkranz, Absorption of microwaves by atmospheric gases, In: Janssen MA, editor. Atmospheric remote sensing by microwave radiometry, Chapter 2. New York: Wiley; 1993.

[19] Liebe HJ. MPM—an atmospheric millimeter-wave propagation model. International Journal of Infrared and Millimeter Waves 1989;10(6):631–50.